Expanded View Figures

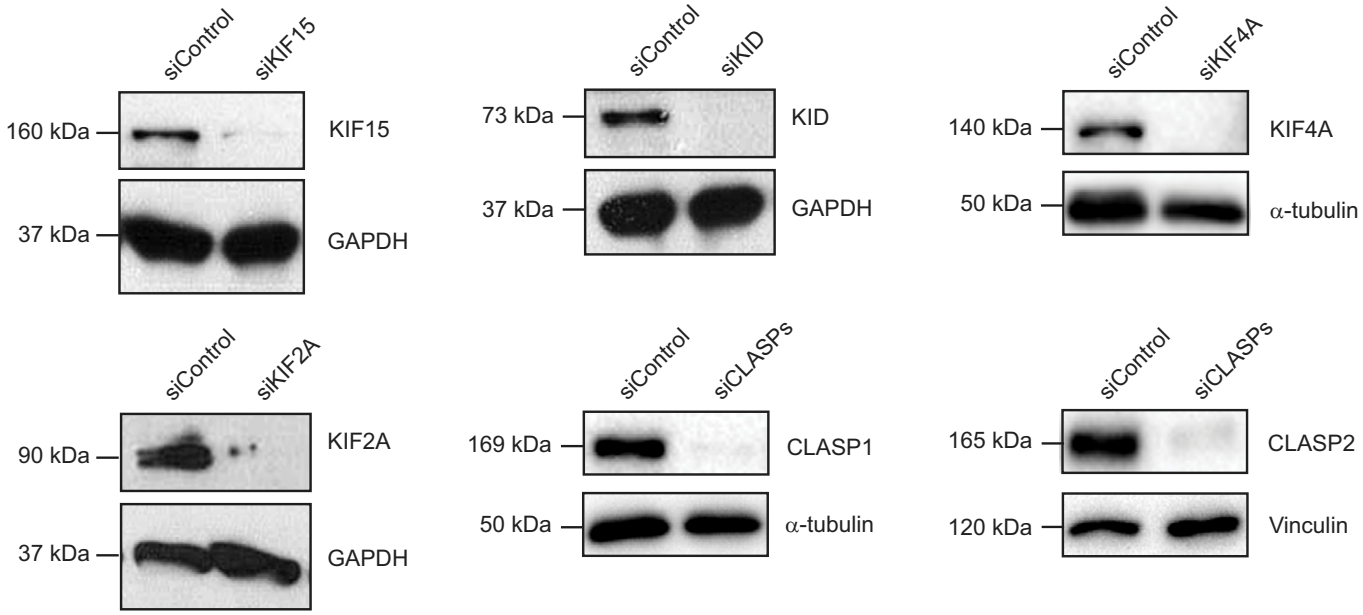

Figure EV1. Efficient RNAi-mediated knockdown of selected MT-flux driving candidates.

Immunoblot analysis of lysates from U2OS cells stably expressing PA-GFP/mCherry-α-tubulin treated with control or indicated siRNAs. Antibodies against respective proteins were used to validate siRNA mediated knockdown, with GAPDH, α-tubulin and vinculin serving as the loading controls.

Figure EV2. Evaluation of localization of KIF4A expression variants and the effect of KIF4A overexpression on MT-flux.

A Immunoblot analysis of cell lysates obtained from U2OS cells stably expressing PA-GFP-α-tubulin infected with different multiplicity of infection (MOI) ratios of mCherry-KIF4A expressing adenovirus. Expression levels of KIF4A upon adenoviral titration were detected using anti-KIF4A antibody, with GAPDH as loading control.

B Quantification of the MT-flux rates upon KIF4A overexpression. The individual values and their mean ± SD are plotted. *N* (number of cells, number of independent experiments): Control (untreated) (23, 3); 1 MOI (33, 3); 2 MOI (26, 3), 4 MOI (9, 1). *P*-values were calculated using Mann–Whitney *U*-test. $^{**}P \leq 0.01$, $^{****}P \leq 0.0001$.

C Representative spinning disk confocal live-cell imaging time series images of U2OS PA-GFP-α-tubulin cells conditionally co-expressing KIF4A shRNA and RNAi-resistant mCherry-KIF4A variants induced using doxycycline. Chromosomes were stained using SiR-DNA. Scale bars, 10 μm. Time, h:min.

D Schematic model illustrating KIF4A-mediated forces in MT-flux driving. Forces exerted by KIF4A motors promote motion of chromosomes relative to MTs. Once a bi-oriented chromosome aligns at the metaphase plate, KIF4A forces can no longer do work on it. Rather, the reactive force on MTs may promote non-KT-MTs to flux toward the poles.

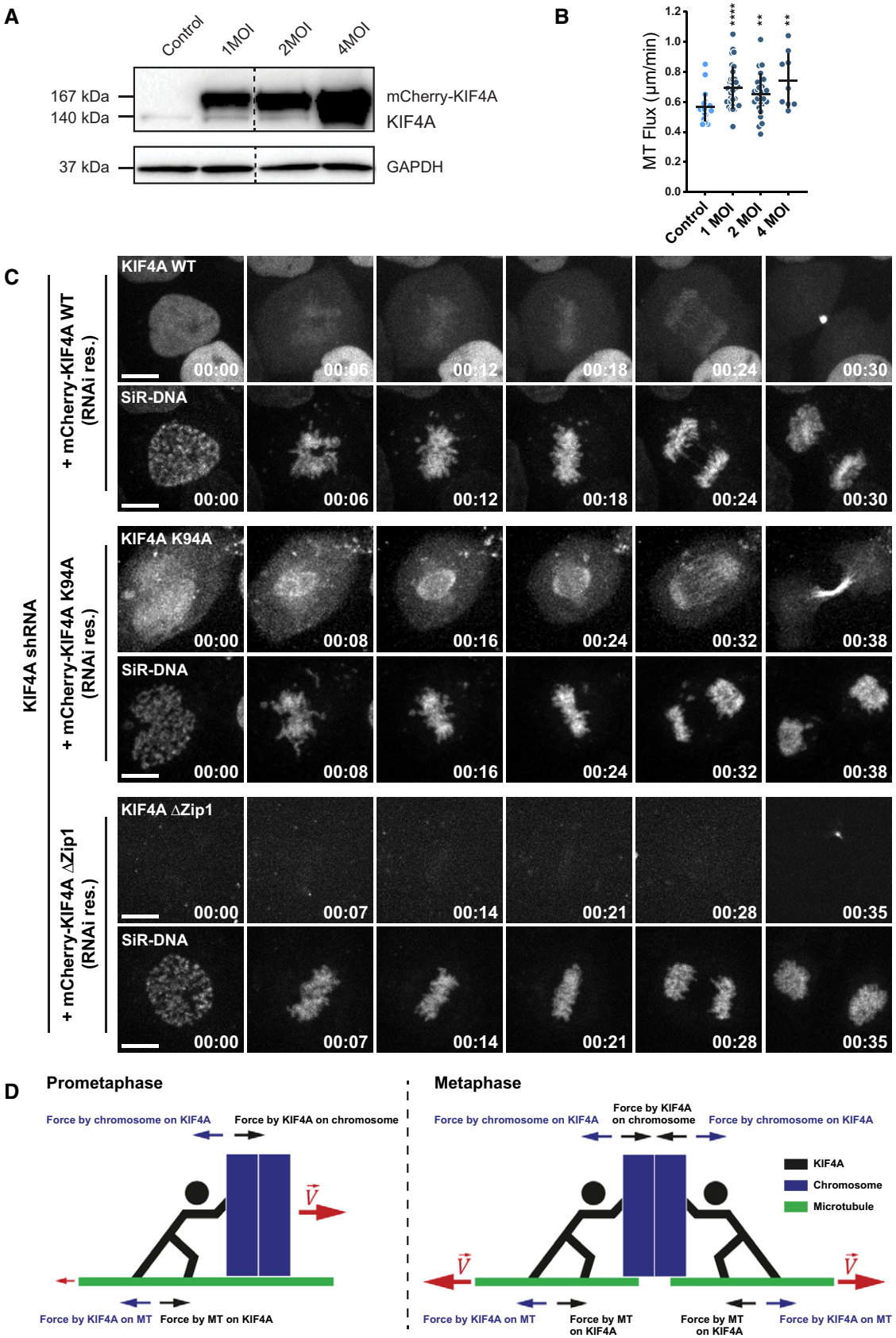

Figure EV2.

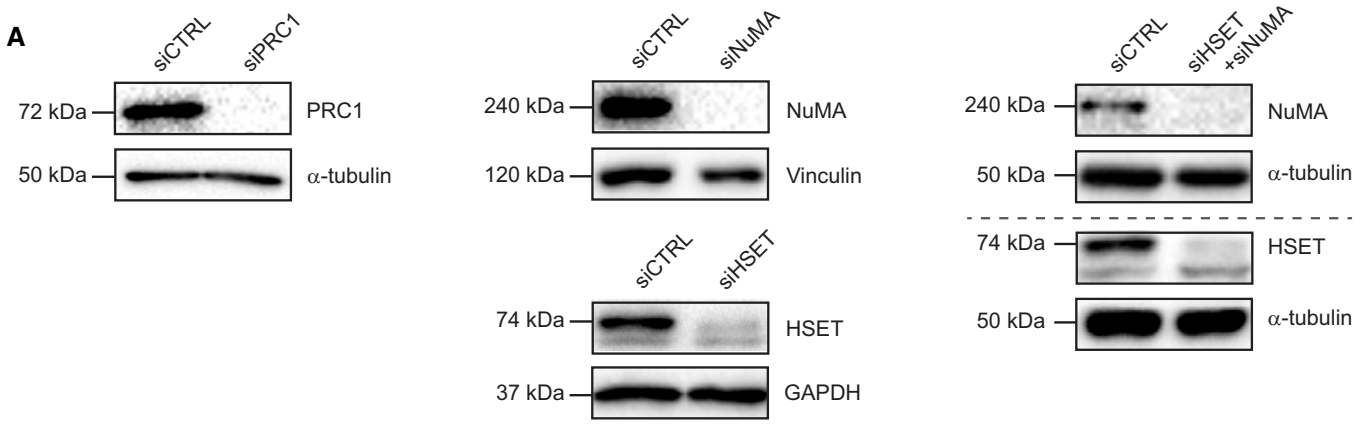

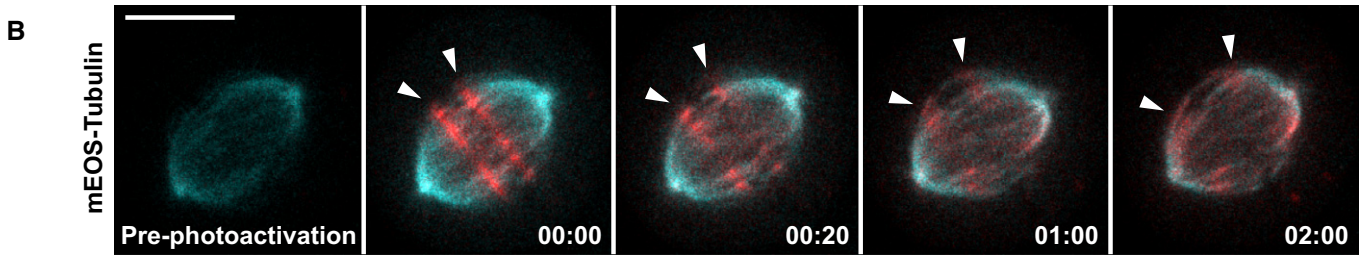

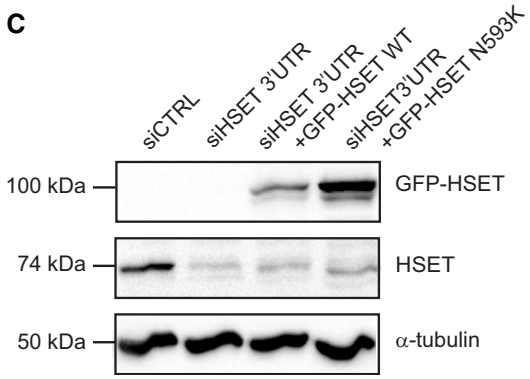

Figure EV3. Analysis of the roles of MT-crosslinking proteins NuMA, HSET and PRC1 in MT-flux.

A Immunoblot analysis of the respective knockdown efficiencies in U2OS cells stably expressing PA-GFP/mCherry-α-tubulin treated with control or indicated siRNAs. GAPDH, α-tubulin and vinculin were used as a loading control.

B Spinning disk confocal time series images of photoconverted mEOS-α-tubulin (red) in U2OS cells stably expressing mEOS-α-tubulin (cyan). White arrowheads highlight the photoconverted regions fluxing toward the poles. Scale bar, 10 μm. Time, min:s.

C Immunoblot analysis of U2OS cells stably expressing mEOS-α-tubulin transfected with control or HSET 3′UTR-targeting siRNAs and co-transfected with the RNAi-resistant GFP-HSET constructs. Expression levels of HSET was observed using anti-HSET antibody with α-tubulin serving as the loading control.

Figure EV4. Analysis of CENP-E contribution to MT-flux in the absence of stable end-on KT-MT attachments.

A Immunoblot analyses of the efficiency of knockdown from U2OS cells stably expressing PA-GFP/mCherry-α-tubulin treated with control or indicated siRNAs, with GAPDH or α-tubulin used as the loading control.

B Representative point-scanning confocal maximum intensity projections of control, STLC-treated and MUGs mitotic spindles in U2OS cells, immunostained with antibodies against CENP-E and α-tubulin. DNA was counterstained with DAPI. CENP-E in red, α-tubulin in green and DNA in blue in merged image. Scale bar, 10 μm.

C CH-STED analyses of HeLa cells stably expressing CENP-E-GFP treated with STLC to induce the formation of monopolar spindles. A top view and a side view of different monopolar spindles are shown. Chromosomes (confocal mode only) were revealed in the larger panels with DAPI (cyan) and MTs (magenta) were detected with an anti-α-tubulin antibody. Arrows indicate examples of clear MT bundles. Scale bar in all panels is 5 μm.

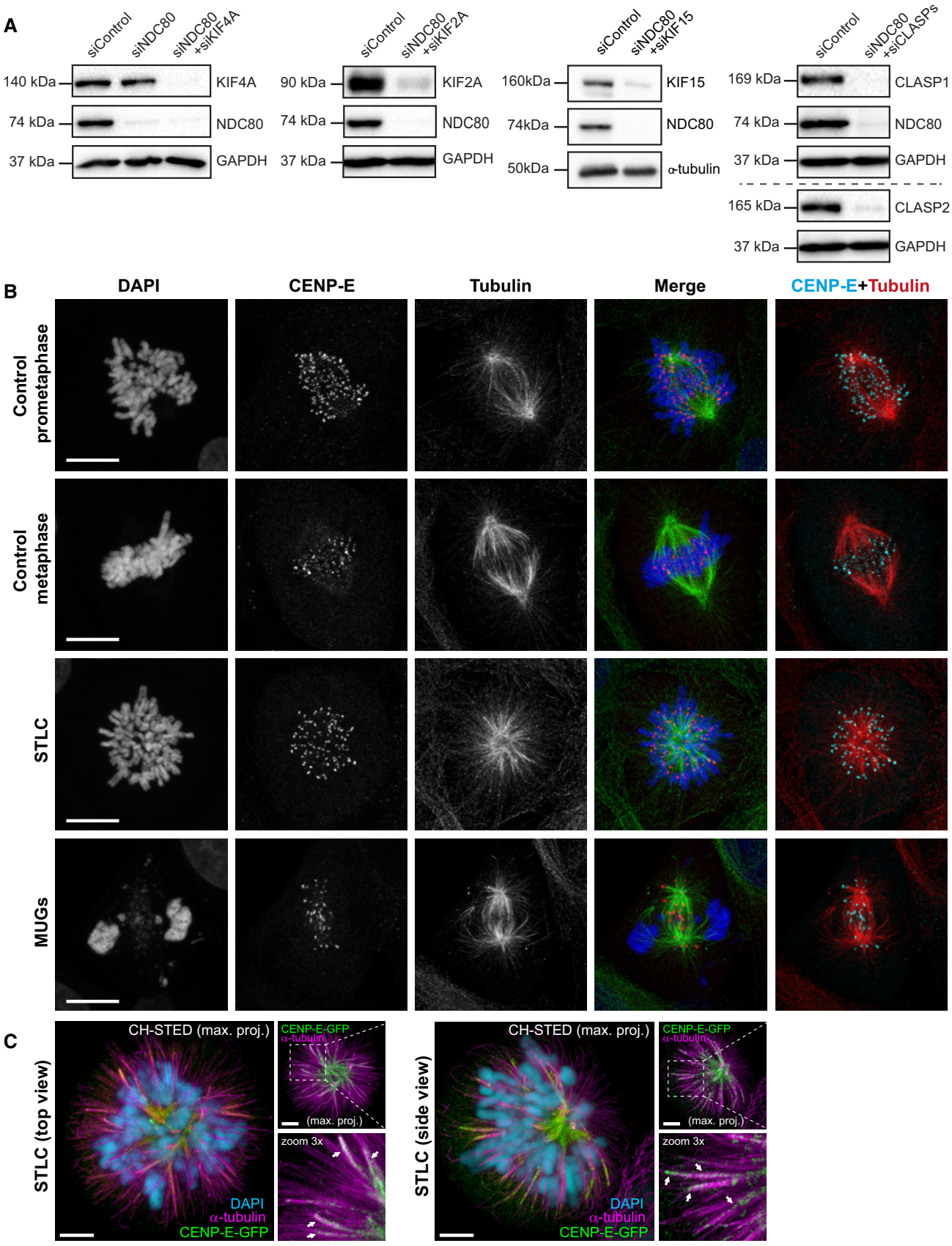

Figure EV4.

Figure EV5. Distribution of antiparallel interpolar MTs during mitosis.

A Representative spinning disk confocal time series of MT-flux during prometaphase (upper panel) and metaphase (lower panel) in U2OS cells stably co-expressing PA-GFP-α-tubulin (cyan) and mCherry-α-tubulin (red), with chromosomes labeled using SiR-DNA (gray). White arrowheads highlight that the photoactivated regions in prometaphase split and move toward both poles (upper panel), whereas metaphase spindles flux uniformly toward individual poles (lower panel). Scale bars, 10 μm. Time, min:s.

B Representative maximum projections of point-scanning confocal immunofluorescence images of prometaphase and metaphase spindles in U2OS cells, stained using antibodies against PRC1 and α-tubulin. DNA was counterstained with DAPI. PRC1 (cyan) and α-tubulin (red) are shown in merged image. The white line signifies area of PRC1-stained antiparallel MTs within the spindle. Scale bar, 10 μm.

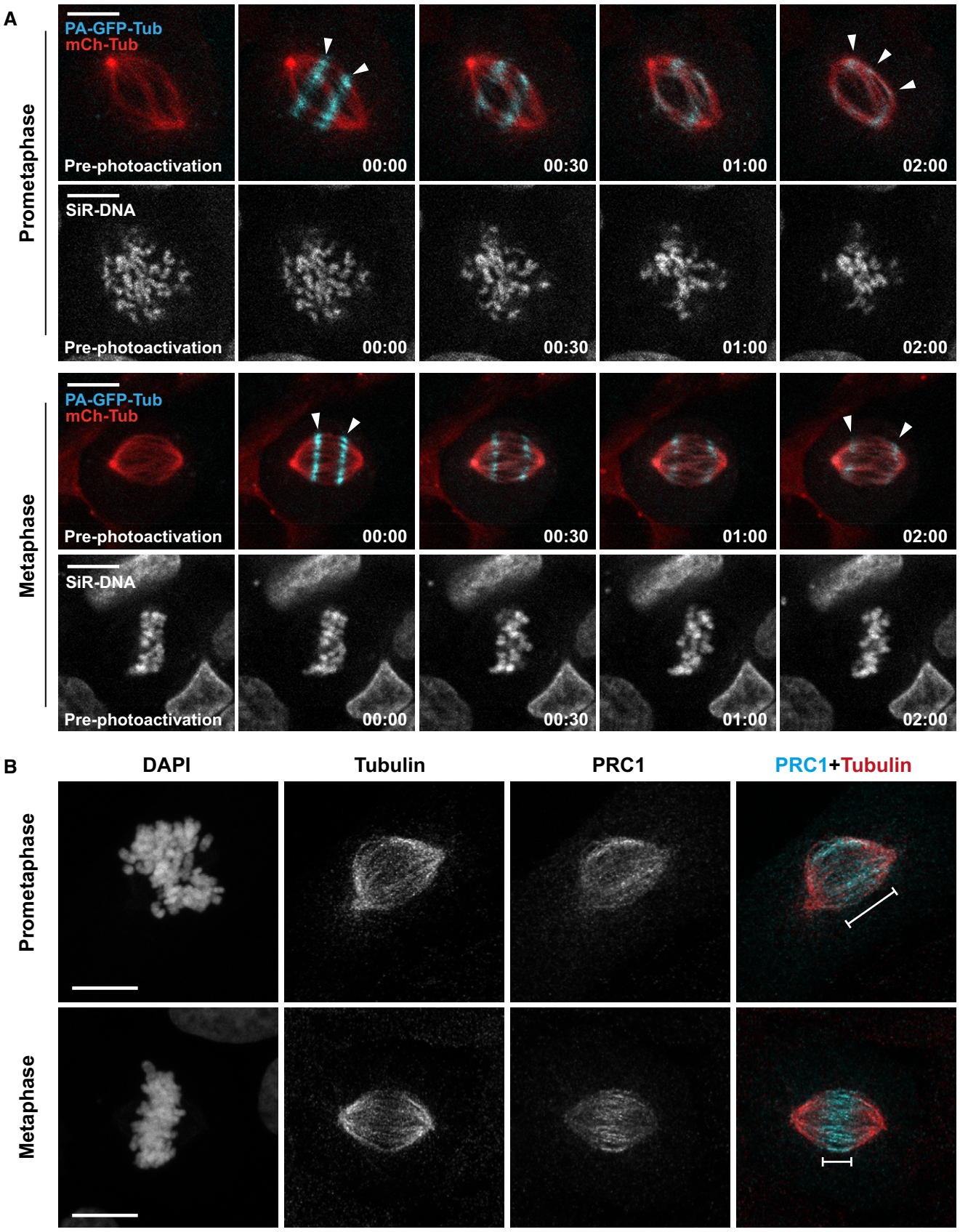

Figure EV5.

Figure EV6. CENP-E localization on interpolar MTs depends on PRC1.

A Representative spinning disk confocal live-cell time series of control and PRC1-depleted HeLa cells stably expressing CENP-E-GFP. White arrowheads highlight CENP-E-GFP at KTs, white arrows highlight CENP-E-GFP on interpolar MTs. Scale bar, 10 μm. Time, h:min.

B Representative point-scanning confocal immunofluorescence images of U2OS cells, stained using antibodies against PRC1 and CENP-E. PRC1 (red) and CENP-E (cyan) are shown in merged image. DNA was counterstained with DAPI. Scale bar, 10 μm. White arrows highlight CENP-E on interpolar MTs.

C Quantification of the impact of PRC1 depletion versus CENP-E inhibition on MT-flux in NDC80-depleted cells. MT-flux values are plotted with mean ± SD. *P*-values were calculated using Mann–Whitney *U*-test. ****$P \leq 0.0001$. siControl, siNDC80 and siNDC80 + GSK923295 data are from Figs 1E and 5B. *N* (number of cells, number of independent experiments): siNDC80 + siPRC1 (37, 3).

D Immunoblot analyses of the efficiency of knockdown from U2OS cells stably expressing PA-GFP/mCherry-α-tubulin treated with control or indicated siRNAs, with α-tubulin used as a loading control.

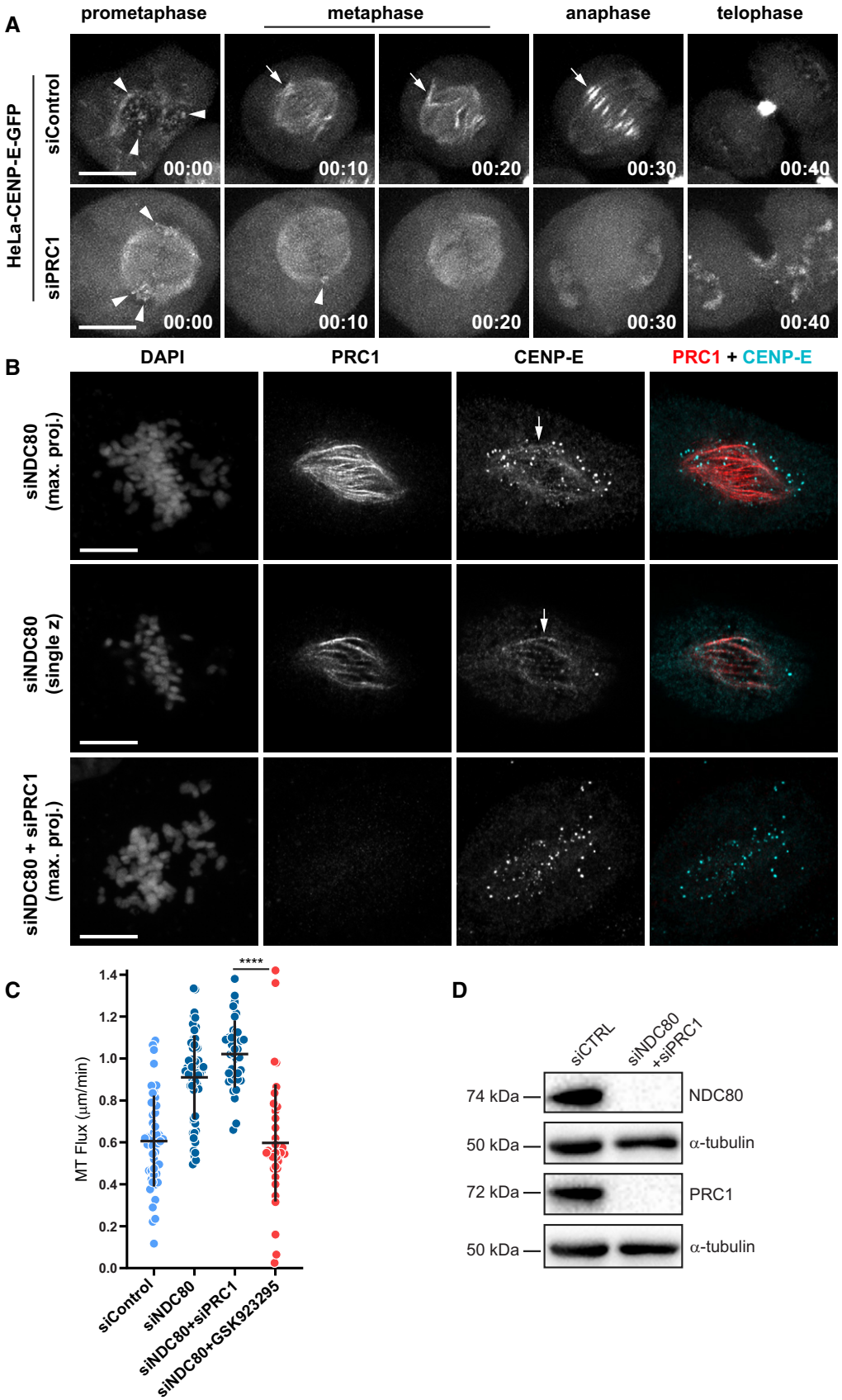

Figure EV6.

Figure EV7. MT-flux counterbalances MCAK activity to maintain spindle length.

A Illustration of the relationship between MT-flux and spindle length in the presence or absence of stable KT-MT end-on attachments.

B Percentage of cells where bipolar spindle collapses to become monopolar after indicated treatments. *N* (number of cells, number of independent experiments): siKIF4A + siKIF15 + STLC (80, 6), siKIF4A + siKIF15 + STLC + siMCAK (94, 3), siKIF4A + siKIF15 + STLC + siKIF2A (37, 3). Graph represents the mean values of individual experiments ± SD. *P*-values were calculated using Student's *t*-test. $^{**}P \leq 0.01$, n.s.—not significant.

C Quantification of the impact of MCAK-mediated recovery on MT-flux. MT-flux with mean ± SD are plotted. siControl, siKIF4A + siKIF15 + STLC and siCLASPs values are from Figs 1E and 7C. *N* (number of cells, number of independent experiments): siKIF4A + siKIF15 + STLC + siMCAK (11, 3) siCLASPs + siMCAK (14, 3). *P*-values were calculated using Student's *t*-test. n.s.—not significant.

D Immunoblot analysis of the knockdown efficiency of indicated proteins in U2OS PA-GFP/mCherry-α-tubulin cells treated with control or target-specific siRNAs. GAPDH and α-tubulin serve as the loading controls.

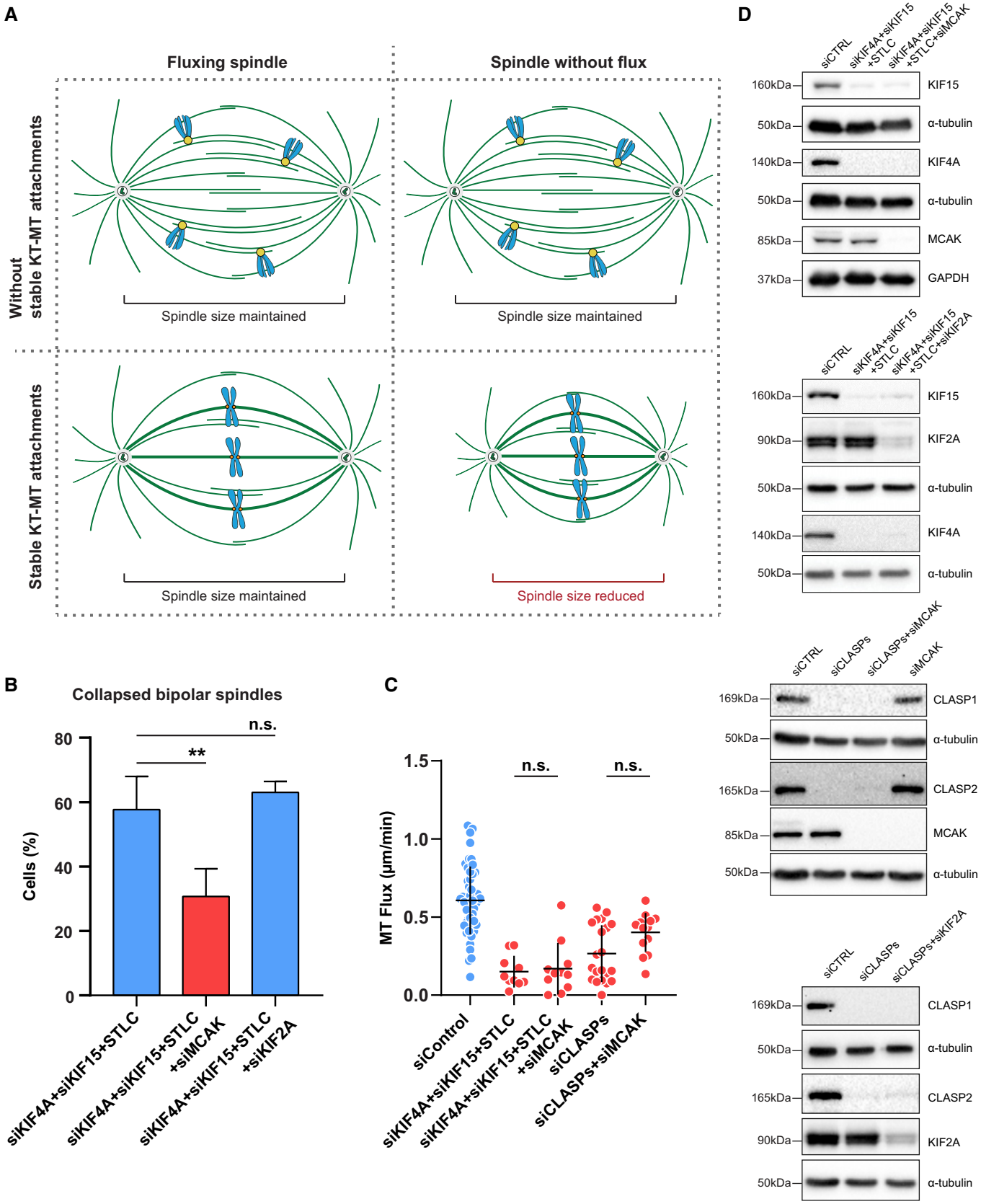

Figure EV7.